Initial Results from the Mini-TES Experiment in Gusev Crater from the Spirit Rover

P. R. Christensen,[1]* S. W. Ruff,[1] R. L. Fergason,[1] A. T. Knudson,[1] S. Anwar,[1] R. E. Arvidson,[2] J. L. Bandfield,[1] D. L. Blaney,[3] C. Budney,[3] W. M. Calvin,[4] T. D. Glotch,[1] M. P. Golombek,[3] N. Gorelick,[1] T. G. Graff,[1] V. E. Hamilton,[5] A. Hayes,[6] J. R. Johnson,[7] H. Y. McSween Jr.,[8] G. L. Mehall,[1] L. K. Mehall,[1] J. E. Moersch,[8] R. V. Morris,[9] A. D. Rogers,[1] M. D. Smith,[10] S. W. Squyres,[6] M. J. Wolff,[11] M. B. Wyatt[1]

The Miniature Thermal Emission Spectrometer (Mini-TES) on Spirit has studied the mineralogy and thermophysical properties at Gusev crater. Undisturbed soil spectra show evidence for minor carbonates and bound water. Rocks are olivine-rich basalts with varying degrees of dust and other coatings. Dark-toned soils observed on disturbed surfaces may be derived from rocks and have derived mineralogy (±5 to 10%) of 45% pyroxene (20% Ca-rich pyroxene and 25% pigeonite), 40% sodic to intermediate plagioclase, and 15% olivine (forsterite 45% ±5 to 10). Two spectrally distinct coatings are observed on rocks, a possible indicator of the interaction of water, rock, and airfall dust. Diurnal temperature data indicate particle sizes from 40 to 80 μm in hollows to ~0.5 to 3 mm in soils.

The Miniature Thermal Emission Spectrometer (Mini-TES) has provided remote measurements of mineralogy, thermophysical properties, and atmospheric temperature profile and composition of the scene surrounding the Spirit rover. The mineralogy of volcanic rocks constrains the composition, depth, and degree of partial melting of their source regions (*1*). Carbonates, evaporites, and oxides provide information on the role of water in the surface evolution. Oxides, such as crystalline hematite, provide insight into aqueous weathering processes, as would the occurrence of clay minerals and other weathering products. The particle size and subsurface layering provide clues to the origin of surficial materials through rock disintegration, aeolian transport, atmospheric fallout, or induration. Mini-TES spectra have also been used to determine the temperature profile in the lower boundary layer, providing evidence for convective activity, and have determined the seasonal trends in atmospheric temperature and dust and cloud opacity.

Mini-TES is a Michelson interferometer that collects infrared spectra from 5 to 29 μm (339 to 1997 cm^{-1}) at a spectral sampling of 10.0 cm^{-1} (*2*). Nominal spatial resolution is 20 mrad; an actuated field stop can be used to reduce the field of view to 8 mrad. The radiometric precision of the instrument is similar to prelaunch precision (*2*, *3*). Spectra were acquired with 2 to 200 spectra summed for a single pointing location, together with 5 to 100 spectra summing for the calibration targets, to increase the radiometric precision by $\sqrt{n}$. Target temperature was determined by fitting a Planck function to the calibrated radiance, giving a temperature precision and accuracy of ±0.5 K and ±2 K, respectively, for typical nighttime and ±0.1 K and ±0.5 K for daytime measurements.

A full 360°, 20-mrad Mini-TES mission success panorama was acquired before egress from the Columbia Memorial Station (Fig. 1) (*4*). Mini-TES rasters with three by three pointing locations were collected regularly along with coregistered 13-filter Panoramic Camera (Pancam) images (*5*) during rover traverses to sample surface diversity. Many other rasters of various sizes and dwell lengths have been acquired, tailored to the requirements of targeted observations. The largest rocks at the Gusev crater site are typically <0.4 m in their largest dimension (*6*), and the hole produced by the Rock Abrasion Tool (RAT) is only 4.5 cm in diameter, or about one-third the size of the ~12-cm Mini-TES field of view directly in front of the rover (*7*). Several targets have been observed with the use of 5× spatial oversampling and spatial deconvolution techniques to improve spectral isolation (*8*), together with multiple RAT brushings to clean larger areas.

Undisturbed surficial materials. Undisturbed surfaces in the vicinity of the station are ~5% surface cover of clasts that range in size from ~1 to 40 cm (*6*), with the remainder composed of finer-grained materials (<100 μm to 3 mm), all coated with a veneer of bright dust (*4*, *9*, *10*). Mini-TES spectra of these surfaces closely match Mars Global Surveyor (MGS) TES spectra of the bright fine-grained dust that blankets low-thermal-inertia regions such as Tharsis and Arabia (Fig. 2) (*11*, *12*). By inference from the analysis of MGS TES spectra (*11*), the Mini-TES spectra of undisturbed materials contain an 840-cm^{-1} (11.9 μm) silicate transparency feature that is best matched by the framework silicates plagioclase feldspar (*11*), zeolite (*13*), or crystalline silica (*14*). These spectra also exhibit the spectral character near 1640 cm^{-1} (6.1 μm) of bound water within a transparent silicate matrix. A third spectral component centered near 1480 cm^{-1} (6.75 μm) is interpreted as due to minor (<5% by weight) carbonate, although other components have also been suggested (*15*). Carbonates produce strong emission when embedded within a silicate matrix that is nearly transparent in this spectral region. The 1480 cm^{-1} absorption corresponds well to the 1450- to 1500-cm^{-1} bands seen in finely particulate anhydrous carbonates (*11*) and most closely matches that of the Mg-carbonate magnesite (*11*). Mini-TES spectra contain absorption by atmospheric CO_2 near 15 μm (*16*) that increases roughly linearly with target distance; this spectral region is excluded in all surface analyses.

The relative mineral abundance of the entire scene from the station to the horizon was mapped with the use of a linear least squares deconvolution (*17*–*20*) of each spectrum acquired in the mission success panorama with a 40-component end-member library constructed from laboratory minerals and MGS TES and Mini-TES surface dust spectra (*21*, *22*). Airfall

[1]Department of Geological Sciences, Arizona State University, Tempe, AZ 85287, USA. [2]Department of Earth and Planetary Sciences, Washington University, St. Louis, MO 63130, USA. [3]Jet Propulsion Laboratory, California Institute of Technology, Pasadena, CA 91109, USA. [4]Department of Geological Science, University of Nevada Reno, NV 89557, USA. [5]Institute of Geophysics and Planetology, University of Hawaii, Honolulu, HI 96822, USA. [6]Department of Astronomy, Space Sciences Building, Cornell University, Ithaca, NY 14853, USA. [7]U.S. Geological Survey, Flagstaff, AZ 86001, USA. [8]Department of Earth and Planetary Sciences, University of Tennessee, Knoxville, TN 37996, USA. [9]National Aeronautics and Space Administration (NASA) Johnson Space Center, Houston, TX 77058, USA. [10]NASA Goddard Space Flight Center, Greenbelt, MD 20771, USA. [11]Space Science Institute, Martinez, GA 30907, USA.

*To whom correspondence should be addressed. E-mail: phil.christensen@asu.edu

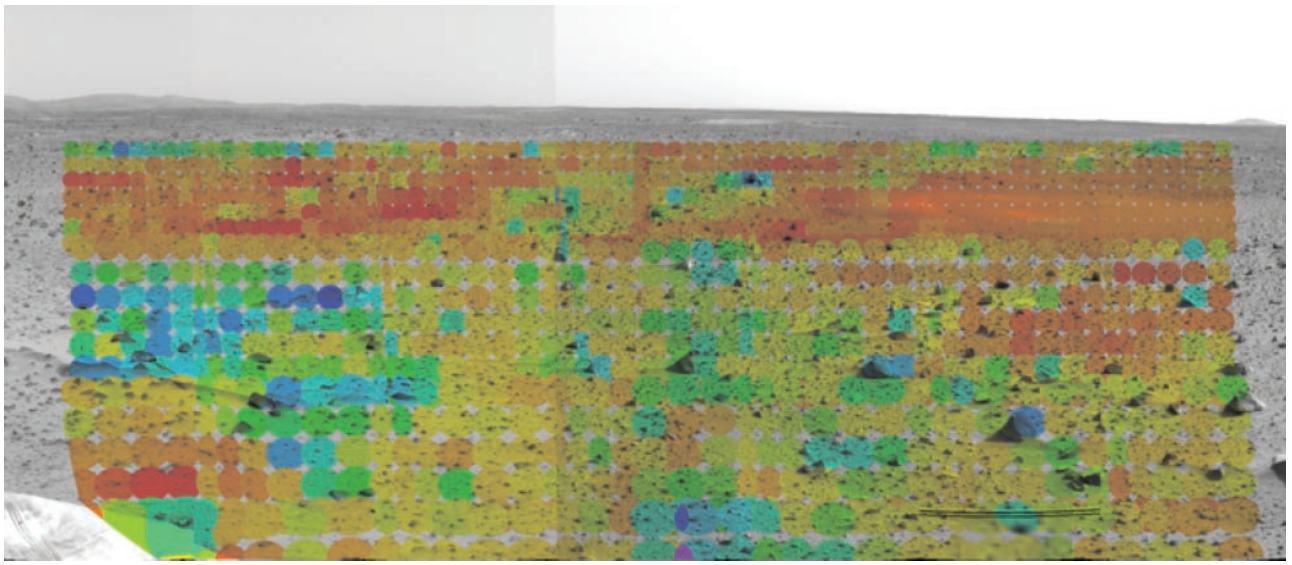

Fig. 1. Temperature image of a portion of the mission success pan. Each Mini-TES pointing location is shown projected onto the initial navcam panorama. Minimum temperature (blue) is 240 K; maximum temperature (red) is 290 K.

dust is ubiquitous at Gusev crater, with all rocks and undisturbed soils (*23*) exhibiting dust spectral features. The 1- to 13-m-diameter hollows only display the spectral features of airfall dust. Variations in undisturbed soil spectra observed through sol 90 (*24*) are primarily because of variable dust content together with differing viewing geometries and target orientations; no systematic compositional variations have been identified.

Disturbed subsurface soil. Mini-TES observed disturbed soils exposed in the rover tracks and trenching operations throughout Spirit's traverse (*4*, *10*). Disturbed soil spectra are similar to low-albedo surface spectra derived from orbit by MGS TES (*25*, *26*), with only minor added features consistent with airfall dust. The distinct spectral differences from dust suggest that dust is a relatively thin veneer and only a minor component of the bulk soil. Linear deconvolution of Mini-TES spectra of rover tracks indicates a basaltic soil, with a composition, normalized to remove the spectral contribution from airfall dust, of ~45% pyroxene (25% pigeonite and 20% clinopyroxene), ~40% sodic to intermediate plagioclase, and ~15% olivine (*27*) (Fig. 3). No goethite was detected, and the magnetite abundance was <5%. The Mini-TES–derived abundances are estimated to have accuracies of ~±5 to 10% on the basis of similar analyses of laboratory and MGS TES rock and mineral mixtures (*17*–*20*, *25*, *28*). The olivine composition of these soils is ~Fo_{45} ± 5 to 10 (*29*), which agrees with α particle x-ray spectrometer (APXS)–derived normative mineralogy (*1*, *30*). This composition is less magnesian than olivine in terrestrial basalts but within the range of martian meteorites (*1*, *31*).

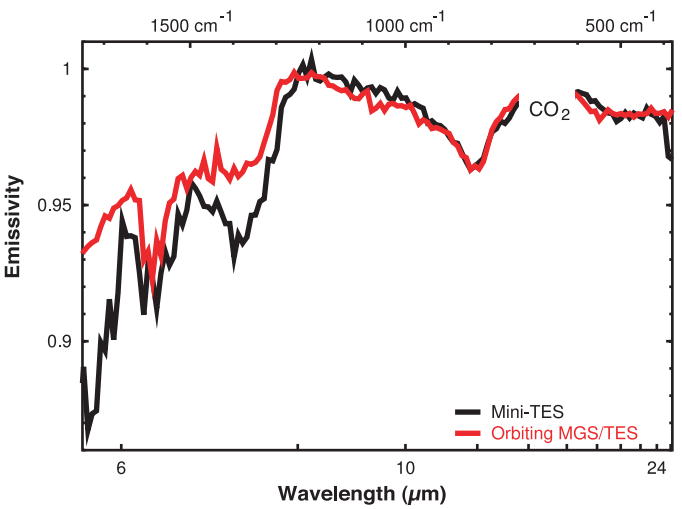

Fig. 2. Mini-TES spectra of the undisturbed soil component compared with an average atmosphere-removed bright-region spectrum from MGS TES (*26*). The deep 840-cm^{-1} feature in both spectra is best matched by a transparency band in framework silicates plagioclase feldspar (*11*), zeolite (*13*), or crystalline silica (*14*). Bound water has a strong emission peak near 1640 cm^{-1}, and carbonates produce strong emission when embedded within a silicate matrix that match the emission peak centered near 1480 cm^{-1}. Both of these features are better defined in the Mini-TES spectra. Mini-TES data are from sol 3, sequence P3004.

The disturbed soil likely gives the best Mini-TES assessment of the bulk mineralogy of Gusev materials. The derived compositions of these soils agree with the compositions of basalts derived from MGS TES, which range from 45 to 50% plagioclase, 25 to 35% Ca-rich pyroxene, 10 to 15% olivine, and 10 to 15% sheet silicates (*25*). The APXS results indicate that the rocks and soil have a similar composition and that the soil is primarily mechanically ground rock that has been loosely consolidated or perhaps mixed with materials from other sources, such as any aqueous-altered materials as suggested by some rinds on rocks (*4*, *30*). Thus, the soil at Gusev is probably derived from local rocks, with only a minor component resulting from airfall dust or surface transport (*4*). In this case, the Mini-TES soil mineralogy is also representative of the rock composition.

Rocks. The rocks at Gusev can be classified as light-toned, dark-toned, and two-toned (*5*). Mini-TES spectra of rocks show a variety of characteristics; representative examples of these spectral types, along with dust and disturbed soil end-members, are shown in Fig. 4. Without exception, the dark-toned rocks and the darker surfaces of two-toned rocks display similar characteristics in Mini-TES spectra (Fig. 5). The two most-studied examples are the 50-cm-wide Adirondack (*32*) and 70-cm-tall Humphrey. The darker, upper portion of these rocks have relatively deep spectral features (emissivity of 0.90 to 0.92) in both the middle (~1300 to 800) and low (<600) wave number regions of

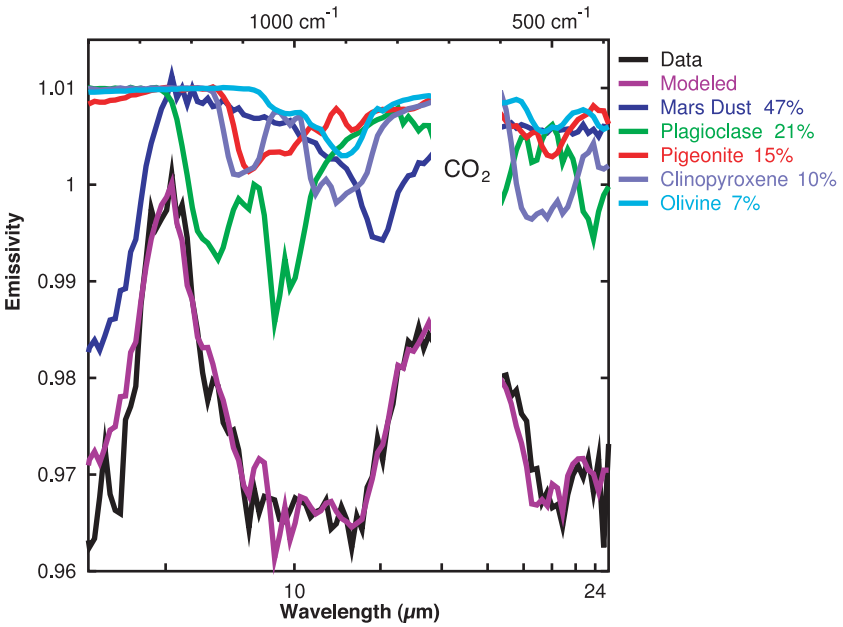

Fig. 3. Mineral components of disturbed soil in a rover track. Mini-TES spectrum is shown compared with the best-fit linear deconvolution model. Data are the average of 200 spectra collected on sol 89, sequence P3660, at 11:01 local solar time with an average target temperature of 267 K.

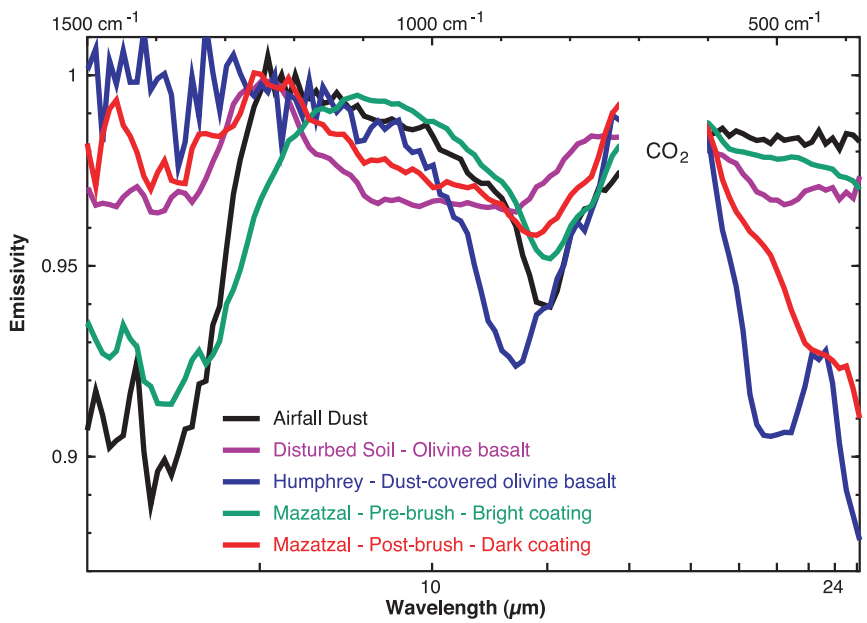

Fig. 4. Representative examples of the primary spectral components observed at Gusev crater.

Mini-TES spectra, whereas the high wave number region (>1300) displays near-unity emissivity (Figs. 4 and 5). Prominent absorptions near 400 and 500 cm^{-1} and the peak at ~450 cm^{-1} are consistent with olivine of intermediate composition (Fo_{35} to Fo_{60}) (Fig. 5), an identification supported by results from the Mössbauer and APXS instruments (*1*, *30*, *33*).

Most of the spectrum, including the prominent absorption feature centered near 880 cm^{-1}, can be well fit by a mixture of olivine and surface dust with lesser pyroxene and oxides (Fig. 6). The fit is poor, however, above 1300 cm^{-1}, where martian dust and laboratory fine-particulate silicates have low emission (*34*). This inconsistency may result from complex radiative transfer effects produced by fine-grained surface material in thermal disequilibrium with the substrate material. Alternatively, there may be a coating of unknown mineralogy on the rocks that is responsible for the 880 cm^{-1} spectral band. Support for this hypothesis comes from the fact that the surfaces of rocks that display the deepest ~880 cm^{-1} band appear to be the darkest and least dusty surfaces observed at the Gusev site, according to Pancam results (*5*).

Excluding the spectral range above 1300 cm^{-1}, the best-fit model spectra of Humphrey and Adirondack contain olivine; pyroxene is only weakly detected, plagioclase is notably absent, and there is dust on the surface (Fig. 6). The best-fit olivine is Fo_{40} to Fo_{45} and falls within the range of martian meteorites and terrestrial basalts (*1*, *31*). The derived oxide abundances are greater than those determined by the APXS and Mössbauer instruments (*1*, *30*, *33*) and may be significantly elevated over the true volumetric abundance because of oxide's possible occurrence as a surface coating.

Light-toned rocks, such as Mazatzal, and the lighter surfaces of two-toned rocks have spectra that are different from dark-toned rocks (Fig. 4). The undisturbed Mazatzal surface has the distinctive spectral characteristics of unconsolidated surface dust, including the emissivity minimum at ~840 cm^{-1}, high, nearly featureless emissivity at low wave numbers, and a low emissivity from 1300 to 1600 cm^{-1} (Fig. 4). However, Mazatzal and most light-toned rocks have an emissivity maximum that is shifted to ~1100 cm^{-1} compared with the maximum at ~1250 cm^{-1} in unconsolidated dust (Fig. 4). This spectral difference between typical airfall dust and the Mazatzal surface suggests the presence of a unique component in the coatings on light-toned surfaces.

The surface of Mazatzal was brushed with the RAT in a pattern of six placements in an effort to remove dust from an area large enough to fill the Mini-TES field of view. The 1100 to 1250 cm^{-1} absorption is no longer present in the brushed-surface spectrum (Fig. 4), indicating that the component that produced this absorption was present in a relatively loose coating that was easily removed by brushing. Microscopic Imager (MI) and Pancam observations of this surface show both a red material, consistent with dust, and a bright material (*5*, *9*) that may be related to the Mini-TES component.

The brushed surface of Mazatzal has deep, broad absorptions from 400 to 600 cm^{-1} that are unique among all Gusev spectra (Fig. 4). The weak absorptions between 900 and 1200 cm^{-1} are similar to those of disturbed soil and are suggestive of basalt (Fig. 4). Absorptions at long wavelengths, but not elsewhere, are characteristic of oxides [e.g., (*35*)]. Deconvolution of the brushed Mazatzal surface gives a mixture of oxides, dust, and plagioclase (fig. S1). Thus, the brushed surface of Mazatzal appears to be a basalt with a relatively thin (<~50 μm) (*36*) oxide coating. MI images of the RAT-abraded surface suggest the presence of a dark, thin coating that differs in texture from the underlying rock (*9*), supporting this hypothesis. The two-toned rock Humphrey was also brushed, with the only significant change being a decrease in spectral contrast. Thus, if dust contributes to

the spectral character of this rock, then sufficient dust must have remained on its surface (*37*, *38*) and within the Mini-TES field of view for the spectral shape to be unchanged.

In summary, the Mini-TES spectra of rocks at Gusev can be tentatively explained by four components: (i) an underlying olivine basalt; (ii) a durable coating or rind, possibly oxide, with deep absorptions from 400 to 600 cm^{-1} that is present on at least one rock (Mazatzal) but not present on all; (iii) a component present in the bright, readily removed coatings on light-toned rocks; and (iv) the ubiquitous unconsolidated airfall dust. The observed spectral characteristics that this model does not explain are the lack of the short wavelength absorption characteristic of dust in some rocks that otherwise appear to have a dust coating and the lack of any significant change in the spectral shape of Humphrey after its brushing.

The occurrence of coatings and rinds of unique mineralogy suggests that some degree of surface alteration has occurred. One possibility is that these rocks have been buried to modest depth, possibly by airfall dust that is periodically deposited and removed by climate variations, and that the alteration is related to the interaction of dust and water films during and/or between periods of burial (*4*, *10*, *39*, *40*). Although Spirit landed in an apparent dust-devil streak with lower albedo than its surroundings (*5*), Gusev crater overall has high albedo and tens of micrometers of dust cover (*34*, *41*), consistent with the ubiquitous presence of dust and coatings observed by Spirit. There is no evidence from orbital mid-infrared spectral observations of similar coatings on surfaces of classic dark regions, such as Syrtis Major, which are interpreted to be unweathered to weakly altered volcanic materials (*25*, *42*, *43*). Rocks in low-albedo regions may lack significant coatings because they have not undergone burial or surface alteration or may have been exposed to aeolian abrasion. Thus, the rocks at Gusev, although consistent with the compositions determined for the basaltic surface type (*1*, *25*), may have a undergone minor surface alteration that was different from their counterparts in low-albedo regions. The presence of both unaltered and coated rocks exposed on the martian surface may not reflect a substantially wetter environment but may be due to minor variations in near- or subsurface alteration.

Sand. Dark-toned particulate material has been observed in drift deposits and ripple forms (*4*, *6*, *10*). Although most accumulations of particulate material are dust-covered, some surfaces have been observed that are darker and less dusty, suggesting active removal of dust. One example is the ripple-like drift deposit Armadillo, which is darker on the inferred upwind side relative to the downwind side (*5*, *40*). Spectra from one of the darker sides display absorptions near 400 and 500 cm^{-1}, similar to the inferred olivine feature observed in spectra from the darkest surfaces of rocks (Fig. 7). The spectral range above 1300 cm^{-1} has higher emissivity than that of dust, consistent with the removal of most of the dust on the darker side as compared with the lighter side of the drift. Deconvolution of these spectra gives a composition of roughly equal amounts of plagioclase, clinopyroxene, olivine (~Fo_{40}), and oxide. This composition is consistent with an origin from plagioclase-rich olivine basalt; high oxide abundances may indicate relatively thin surface coatings or aeolian concentrations. The spectra of these materials closely match those of the dark-toned dunes adjacent to the interior wall of Bonneville crater as well as the average atmospherically corrected TES spectrum obtained for the Gusev site, suggesting that this dark drift or dune material occurs throughout the region.

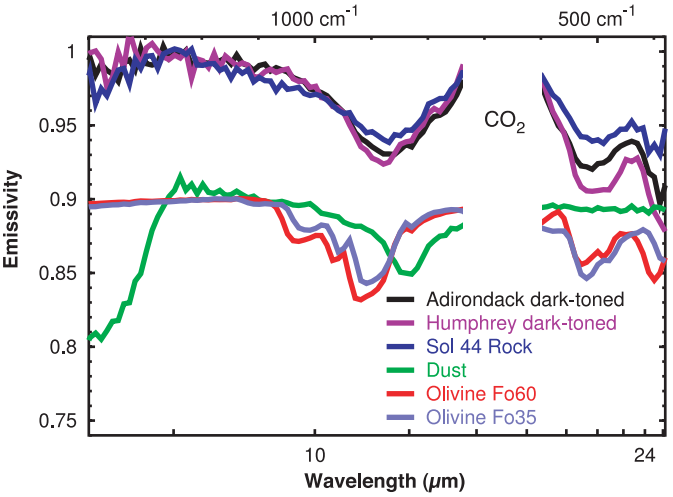

Fig. 5. Mini-TES spectra of Adirondack, Humphrey, and an unnamed rock from sol 44 compared with typical Gusev dust-cover surface and laboratory olivine. Note the similarity of the three rocks to each other and the spectral match to olivine between 21 and 25 μm. The broad rock absorption between 9 and 14 μm can be fit by the combination of olivine and surface dust. Data are from sol 14, sequence P3110; sol 56, sequence P3175; and sol 44, sequence P3625, respectively. Laboratory and dust spectra have been offset for clarity.

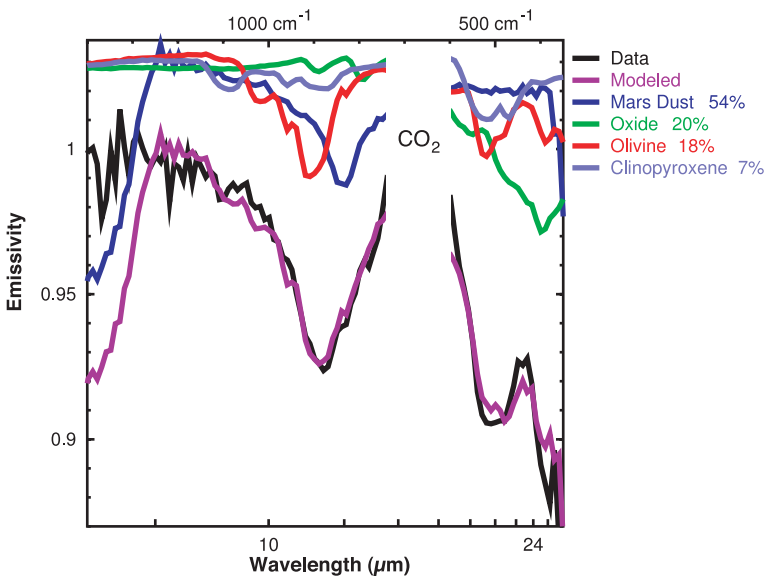

Fig. 6. Quantitative mineral abundance of Humphrey using the linear deconvolution of the Mini-TES spectra with a library of mineral end-members.

Thermophysical properties. Diurnal brightness temperature measurements have been used with a model evolved from that used for Viking Infrared Thermal Mapper (IRTM) (*44*) and MGS TES data analysis (*45*) to derive the thermal inertia and average particle size for drift deposits, hollow fill material, and disturbed soil (Plate 6). Model inputs include a dust opacity of 0.4, derived from Mini-TES and Pancam, and a TES-derived albedo of 0.20 (*43*). Soil thermal inertias range from 150 to 430 J m^{-2} K^{-1} $s^{-1/2}$. The 5-km resolution TES inertia for this location is 290 J m^{-2} K^{-1} $s^{-1/2}$ (*43*), which falls within the range observed in situ. Thermal Emission Imaging System (THEMIS)

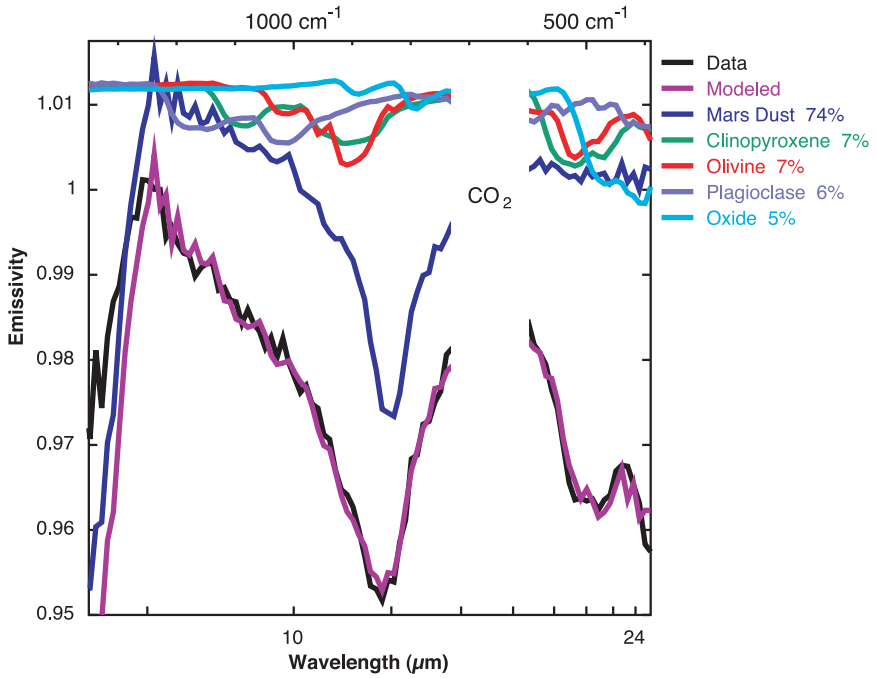

Fig. 7. Quantitative mineral abundance of dark sands in the Armadillo drift using the linear deconvolution of the Mini-TES spectra with a library of mineral end-members. Data are from sol 67, sequence P3143.

orbital data show an elevated thermal inertia of ~450 J m^{-2} K^{-1} $s^{-1/2}$ around Bonneville crater at 100-m scales (*46*) that is consistent with an increase in rock abundance from 5% to a factor of 2 to 4 higher in the crater ejecta (*47*) with no required change in soil properties. The hollows have the lowest inertias observed, 150 to 240 J m^{-2} K^{-1} $s^{-1/2}$, corresponding to an average particle size for well-sorted, unconsolidated particles of silt (40 μm) to medium sand (275 μm) (*48*, *49*). Drift deposits, which include ripples and dunes, have inertias of 300 to 430 J m^{-2} K^{-1} $s^{-1/2}$ (average particle size of ~500 μm to 1 to 3 mm) (*48*–*50*). The traverse from the landing site to Bonneville crater yielded no systematic variation in the thermal inertia of the surface of fine-grained silts to cm-sized stones.

The size-frequency distribution of rocks around the station generally follows the exponential model distribution based on the Viking Lander and MPF landing sites for 5% rock abundance (*51*). The area covered by rocks > 0.1 m diameter is about half of the total, suggesting an insufficient number of rocks large enough at this spot to account for the estimate from analyses of Viking IRTM data (*52*). If this count is representative of the broader area observed from orbit, then the fine-component thermal inertia is probably higher than has been estimated, which is consistent with the pebble-rich and indurated or cemented soil layer or duricrust observed by Spirit (*4*, *6*, *10*). The observed thermal inertias at the surface and particle sizes (including rock coverage) are consistent with those observed and inferred in orbital data and are in agreement with predictions made before landing (*4*, *53*).

References and Notes

1. H. Y. McSween Jr. *et al.*, *Science* **305**, 842 (2004).
2. P. R. Christensen *et al.*, *J. Geophys. Res.* **198**, 1029/2003JE002117 (2003).
3. Two-point radiometric calibration was intended to use two V-groove blackbody targets (*2*). The temperature sensors attached to the rover deck failed at extremely low temperatures (~–90°C) on the first night after landing. The calibration was modified to use prelaunch measurements of the instrument response function taken over temperature, with the instrument radiance determined from observations of the functioning target mounted in the Pancam mast assembly (PMA). On the basis of comparison with orbiting MGS TES data and modeling of the atmospheric observations, the response function has not changed from prelaunch values and the calibration approach is providing the required accuracy. The 1-σ radiometric precision for two-spectra summing is $\pm 1.8 \times 10^{-8}$ W cm^{-2} sr^{-1} cm^{-1} between 450 and 1300 cm^{-1}, increasing to $\sim 7 \times 10^{-8}$ W cm^{-2} sr^{-1} cm^{-1} at shorter (300 cm^{-1}) and longer (1800 cm^{-1}) wave numbers. The absolute radiance error is $< 5 \times 10^{-8}$ W cm^{-2} sr^{-1} cm^{-1}, decreasing to $\sim 1 \times 10^{-8}$ W cm^{-2} sr^{-1} cm^{-1}
4. S. W. Squyres *et al.*, *Science* **305**, 794 (2004).
5. J. F. Bell III *et al.*, *Science* **305**, 800 (2004).
6. J. A. Grant *et al.*, *Science* **305**, 807 (2004).
7. The Mini-TES nominal field of view is 20 mrad at infinity. For near-field observations, the field of view is the aperture diameter (6.35 cm) plus the 20 mrad divergence from the location of the telescope to the point being observed. Targets in the arm work volume are ~1.5 m in front of the rover, giving a total path length of ~3 m from the Mini-TES telescope. The resulting Mini-TES field of view is ~12 cm at the end of the rover arm.
8. S. M. Ciccollela, J. E. Moersch, *Proc. Lunar Planet. Sci.* **XXXIV**, 1836 (2003).
9. K. E. Herkenhoff *et al.*, *Science* **305**, 824 (2004).
10. R. E. Arvidson *et al.*, *Science* **305**, 821 (2004).
11. J. L. Bandfield, T. D. Glotch, P. R. Christensen, *Science* **301**, 1084 (2003).
12. "Dust" is used throughout to indicate the fine-grained component of surface materials with similar spectral character to regional dust deposits observed by MGS TES and interpreted to be air fallout from regional and global dust storms.
13. S. W. Ruff, *Icarus* **168**, 131 (2004).
14. J. L. Bishop, E. Murad, M. D. Lane, R. L. Mancinelli, *Icarus* **169**, 331 (2004).
15. M. D. Lane, *Proc. Lunar Planet. Sci.* **XXXV**, abstr. 1858 (2004) [CD-ROM].
16. M. D. Smith *et al.*, in preparation.
17. M. S. Ramsey, P. R. Christensen, *J. Geophys. Res.* **103**, 577 (1998).
18. K. C. Feely, P. R. Christensen, *J. Geophys. Res.* **104**, 24195 (1999).
19. M. B. Wyatt, V. E. Hamilton, J. H. Y. McSween, P. R. Christensen, L. A. Taylor, *J. Geophys. Res.* **106**, 14711 (2001).
20. V. E. Hamilton, M. B. Wyatt, J. McSween, P. R. Christensen, *J. Geophys. Res.* **106**, 14733 (2001).
21. The mineral suite used for deconvolution included a broad range of pyroxene, feldspar, olivine, oxide, and surface dust compositions. Initial studies included carbonates and sulfates that resulted in somewhat better mathematical fits but at low (<2%) abundances of these minerals that were below detection limits. These minerals were subsequently removed from the library. The fits using only the remaining minerals give somewhat worse root mean square errors but provide a better determination of the abundances of the minerals that are reliably detected.
22. P. R. Christensen *et al.*, *J. Geophys. Res.* **105**, 9735 (2000).
23. The term martian soil is used here to denote any loose, unconsolidated materials that can be distinguished from rocks, bedrock, or strongly cohesive sediments. No implication of the presence or absence of organic materials or living matter is intended.
24. A martian solar day has a mean period of 24 hours 39 min 35.244 s and is referred to as a sol to distinguish this from a roughly 3%-shorter solar day on Earth. A martian sidereal day, as measured with respect to the fixed stars, is 24 hours 37 min 22.663 s, as compared with 23 hours 56 min 04.0905 s for Earth. See http://www.giss.nasa.gov/tools/mars24/ for more information.
25. P. R. Christensen, J. L. Bandfield, M. D. Smith, V. E. Hamilton, R. N. Clark, *J. Geophys. Res.* **105**, 9609 (2000).
26. J. L. Bandfield, M. D. Smith, *Icarus* **161**, 47 (2003).
27. The individual minerals fit to the spectra have been summed into mineral groups.
28. J. L. Bandfield, *J. Geophys. Res.* **107**, 10.1029/2001JE001510 (2002).
29. The Fo (forsterite) value is the amount of FeO in the olivine, where forsterite is the Mg end-member and fayalite is the Fe end-member.
30. R. Gellert *et al.*, *Science* **305**, 829 (2004).
31. H. Y. McSween Jr., A. H. Treiman, in *Planetary Materials*, J. Papike, Ed. (Mineralogical Society of America, Washington, DC, 1998), chap. 6.
32. Names have assigned to areographic features by the Mars Exploration Rover (MER) team for planning and operations purposes. The names are not formally recognized by the International Astronomical Union.
33. R. V. Morris *et al.*, *Science* **305**, 833 (2004).
34. S. W. Ruff, P. R. Christensen, *J. Geophys. Res.* **107**, 10.1029/2001JE001580 (2002).
35. V. C. Farmer, *The Infrared Spectra of Minerals* (Mineralogical Society, London, 1974).
36. P. R. Christensen, S. T. Harrison, *J. Geophys. Res.* **98**, 19819 (1993).
37. J. R. Johnson, P. R. Christensen, P. G. Lucey, *J. Geophys. Res.* **107**, 10.1029/2000JE001405 (2002).
38. T. G. Graff, thesis, Arizona State University, Tempe, AZ (2003).
39. P. R. Christensen, *J. Geophys. Res.* **91**, 3533 (1985).
40. R. Greeley *et al.*, *Science* **305**, 810 (2004).
41. P. R. Christensen *et al.*, in preparation.
42. J. L. Bandfield, V. E. Hamilton, P. R. Christensen, *Science* **287**, 1626 (2000).

43. P. R. Christensen *et al*., *J. Geophys. Res.* **106**, 23823 (2001).
44. H. H. Kieffer *et al*., *J. Geophys. Res.* **82**, 4249 (1977).
45. M. T. Mellon, B. M. Jakosky, H. H. Kieffer, P. R. Christensen, *Icarus* **148**, 437 (2000).
46. R. L. Fergason, P. R. Christensen, *Proc. Lunar Planet. Sci.* **XXXIV**, abstr. 1785 (2003).
47. M. P. Golombek *et al*., *Proc. Lunar Planet. Sci.* **XXXIV**, abstr. 25041 (2004).
48. H. H. Kieffer, J. S. C. Chase, E. Miner, G. Munch, G. Neugebauer, *J. Geophys. Res.* **78**, 4291 (1973).
49. M. A. Presley, P. R. Christensen, *J. Geophys. Res.* **102**, 6551 (1997).
50. K. S. Edgett, P. R. Christensen, *J. Geophys. Res.* **96**, 22,765 (1991).
51. M. P. Golombek *et al*., *J. Geophys. Res.* **108**, 10.1029/2002JE0020235 (2003).
52. P. R. Christensen, *Icarus* **68**, 217 (1986).
53. M. P. Golombek *et al*., *J. Geophys. Res.* **108**, 1029/2003JE002074 (2003).
54. We would like to express our deepest appreciation to all of the individuals at Raytheon Santa Barbara Remote Sensing, led by S. Silverman, and at the Jet Propulsion Laboratory whose effort and dedication have led to the successful acquisition of Mini-TES data from the surface at Gusev Crater. Funding was provided by the MER Project Science Office.

Supporting Online Material
www.sciencemag.org/cgi/content/full/305/5685/837/DC1
Materials and Methods
SOM Text
Fig. S1

Plates Referenced in Article
www.sciencemag.org/cgi/content/full/305/5685/837/DC2
Plate 6

21 May 2004; accepted 7 July 2004

REPORT

Basaltic Rocks Analyzed by the Spirit Rover in Gusev Crater

H. Y. McSween,[1] R. E. Arvidson,[2] J. F. Bell III,[3] D. Blaney,[4] N. A. Cabrol,[5] P. R. Christensen,[6] B. C. Clark,[7] J. A. Crisp,[4] L. S. Crumpler,[8] D. J. Des Marais,[5] J. D. Farmer,[6] R. Gellert,[9] A. Ghosh,[1] S. Gorevan,[10] T. Graff,[6] J. Grant,[11] L. A. Haskin,[2] K. E. Herkenhoff,[12] J. R. Johnson,[12] B. L. Jolliff,[2] G. Klingelhoefer,[13] A. T. Knudson,[6] S. McLennan,[14] K. A. Milam,[1] J. E. Moersch,[1] R. V. Morris,[15] R. Rieder,[9] S. W. Ruff,[6] P. A. de Souza Jr.,[16] S. W. Squyres,[3] H. Wänke,[9] A. Wang,[2] M. B. Wyatt,[6] A. Yen,[4] J. Zipfel[9]

The Spirit landing site in Gusev Crater on Mars contains dark, fine-grained, vesicular rocks interpreted as lavas. Pancam and Mini–Thermal Emission Spectrometer (Mini-TES) spectra suggest that all of these rocks are similar but have variable coatings and dust mantles. Magnified images of brushed and abraded rock surfaces show alteration rinds and veins. Rock interiors contain ≤25% megacrysts. Chemical analyses of rocks by the Alpha Particle X-ray Spectrometer are consistent with picritic basalts, containing normative olivine, pyroxenes, plagioclase, and accessory FeTi oxides. Mössbauer, Pancam, and Mini-TES spectra confirm the presence of olivine, magnetite, and probably pyroxene. These basalts extend the known range of rock compositions composing the martian crust.

Rocks at the Spirit landing site are fine-grained with irregular vesicles and vugs, suggesting a volcanic origin. The rocks are angular and strewn across the surface, which suggests they were ejected from nearby Bonneville crater (*1*) by an impact event (*2*).

Pancam and Mini–Thermal Emission Spectrometer (Mini-TES) spectra of rock surfaces indicate two end members, represented by dark- and light-toned rocks, with most rocks falling between these extremes. Three representative rocks, Adirondack, Humphrey, and Mazatzal, located several hundred meters apart, have been analyzed with the Athena instruments (*3*). Pancam images (*4*) show that Adirondack and Humphrey are partly coated and that Mazatzal is uniformly coated by light-toned material (Plates 9, 11, and 14). Pancam spectra (Fig. 1) of the dark portions of Adirondack and Humphrey are consistent with the presence of olivine, which has a broad (composite) absorption band near 1000 nm. A weak band center near 930 nm suggests the presence of pyroxene or contamination by ferric oxides.

The long-wavelength portion of Mini-TES spectra of dark rock surfaces resembles the Mars Global Surveyor (MGS)–TES spectra of

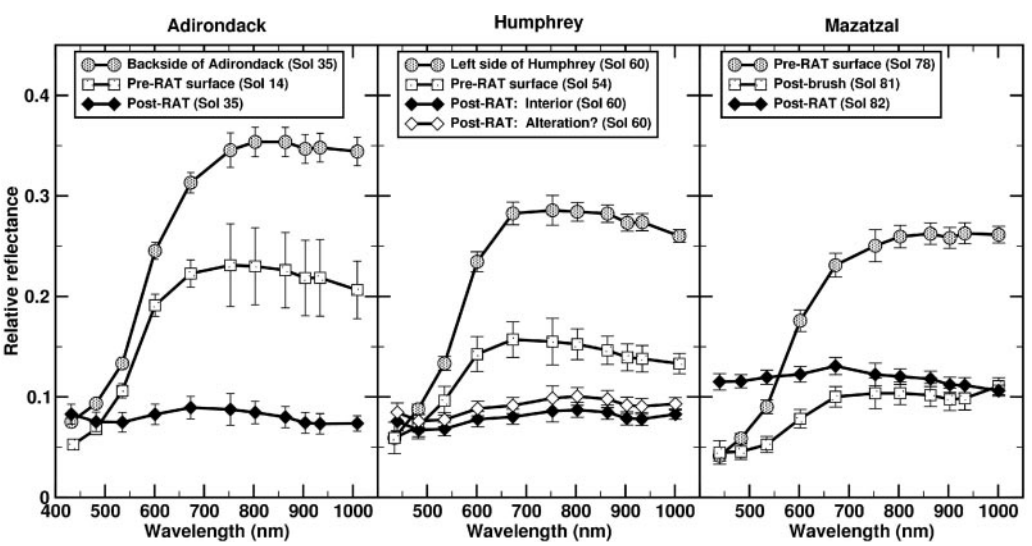

Fig. 1. Relative reflectance Pancam spectra of Adirondack, Humphrey, and Mazatzal (*20*). Dark-toned portions and abraded interiors (post-RAT) of rocks have flat, relatively featureless spectra consistent with basalt.

Initial Results from the Mini-TES Experiment in Gusev Crater from the Spirit Rover

P. R. Christensen *et al.*

Science **305**, 837 (2004);
DOI: 10.1126/science.1100564